Biophysical Journal Volume 105 July 2013 40–47

Measurement of Cationic and Intracellular Modulation of Integrin Binding Affinity by AFM-Based Nanorobot

Kevin C. Patterson,[‡△] Ruiguo Yang,[†△] Bixi Zeng,[‡] Bo Song,[†] Shouye Wang,[§] Ning Xi,[†*] and Marc D. Basson[§*]
[‡]College of Human Medicine, [†]Department of Electrical and Computer Engineering, and [§]Department of Surgery, Michigan State University, East Lansing, Michigan

ABSTRACT Integrins are dynamic transmembrane cation-dependent heterodimers that both anchor cells in position and transduce signals into and out of cells. We used an atomic force microscope (AFM)-based nanorobotic system to measure integrin-binding forces in intact human intestinal epithelial Caco-2 cells. The AFM-based nanorobot enables human-directed, high-accuracy probe positioning and site-specific investigations. Functionalizing the AFM probe with an arginine-glycine-aspartate (RGD)-containing sequence (consensus binding sequence for integrins) allowed us to detect a series of peptide-cell membrane interactions with a median binding force of 115.1 ± 4.9 pN that were not detected in control interactions. Chelating divalent cations from the culture medium abolished these interactions, as did inhibiting intracellular focal adhesion kinase (FAK) using Y15. Adding 1 mM Mg^{2+} to the medium caused a rightward shift in the force-binding curve. Adding 1 mM Ca^{2+} virtually abolished the RGD-membrane specific interactions and blocked the Mg^{2+} effects. Cell adhesion assays demonstrated parallel effects of divalent cations and the FAK inhibitor on cell adhesion. These results demonstrate direct modulation of integrin-binding affinity by both divalent cations and intracellular signal inhibition. Additionally, three binding states (nonspecific, specific inactivated, and specific activated) were delineated from affinity measurements. Although other research has assumed that this process of integrin conformational change causes altered ligand binding, in this work we directly measured these three states in individual integrins in a physiologically based study.

INTRODUCTION

Integrins are cation-dependent transmembrane dimers that interact with extracellular matrix (ECM) proteins such as collagen, fibronectin, vitronectin, and laminin. Integrins are important for cell functions such as migration or embryogenesis, and in pathophysiologic events as diverse as leukocyte adhesion during inflammation or infection, blood clotting, and cancer. Alterations in the functional status of integrins in cancer facilitate metastasis (1,2). These adhesion structures are heterodimeric proteins with diverse α and β subunits. The specific subunit composition of each integrin determines its functionality and specificity (3). Integrins anchor the cell to the ECM and in some cases to other cells, and transduce signals defined by the ECM composition and organization into the cell (3), as well as signals initiated by deformation of the matrix (4). An amino acid triplet containing arginine, glycine, and glutamate is a vital consensus feature of proteins bound by many integrin heterodimers, including $\alpha5\beta1$, $\alpha8\beta1$, $\alpha V\beta1$, $\alpha V\beta3$, $\alpha V\beta5$, $\alpha V\beta6$, $\alpha V\beta8$, and $\alpha IIb\beta3$ (5–8).

The binding ability of integrins is state dependent, with an open or closed conformation that is classically believed to depend largely on the occupancy of an extracellular divalent cation-binding site. Mg^{2+} and Mn^{2+} are believed to maintain integrins in an open status, enabling them to bind to other structures, whereas Ca^{2+} and Zn^{2+} have been hypothesized to stimulate a closed conformation that limits binding interactions (9–11). Although these changes in ligand-binding force by individual integrins determine affinity, clustering of integrins can increase the overall binding force, which is described as a change in avidity. Although integrins were originally thought to transduce signals primarily from outside the cell, it is now becoming increasingly clear that both affinity (12) and avidity (2,13) may be influenced by intracellular signaling, allowing signals from within the cell to affect external events. Several intracellular proteins, such as focal adhesion kinase (FAK) (14,15), congregate around the cytoplasmic domain of integrins, forming focal adhesions. FAK is important in regulating the functional status of integrins and mediating cell adhesion and migration, and even plays a role in cancer progression and metastasis (16–18). FAK also interacts with many other molecules inside the cell and is therefore a target for signaling and medical research (14,18,19).

The atomic force microscope (AFM) has been used in biology to characterize and interact with living cells. It utilizes an ultrasharp tip attached to an accurately position-controlled cantilever. Physical interactions between the sample and the tip can be detected by the bending of the cantilever. Thus, the AFM can be used to obtain topographical information down to the nanoscale. It has been used to image structures and characterize the mechanical properties of living cells. Additional functional capability is introduced by attaching the tip with various chemical reagents to probe surface interactions (20–23). In previous studies, investigators used AFM to measure the cell-ECM interface (24) and

Submitted February 19, 2013, and accepted for publication May 30, 2013.
△Kevin C. Patterson and Ruiguo Yang contributed equally to this work.
*Correspondence: xin@egr.msu.edu or marc.basson@hc.msu.edu
Edtior: Levi Gheber.

0006-3495/13/07/0040/8 $2.00
http://dx.doi.org/10.1016/j.bpj.2013.05.052

integrin interactions (25,26) in living cells in various cell lines. However, these authors did not conduct physiologically relevant experiments and did not alter the properties of integrin binding because they utilized features such as temperature outside of human limits.

Previous studies have approached the concept of integrin-binding affinities on a statistical and global level (10,27). AFM permits more specific assessment at the molecular level of interaction. Integrin interactions with glycine-arginine-glycine-aspartate-serine-proline (RGD)-containing proteins were previously characterized by Sun and colleagues (25) using AFM, but no adjustment of the cell environment was performed in that study. Lehenkari and Horton (26) also used AFM to assess the integrin-RGD binding force, but mainly altered the pH of the environment between 7.4 and 4.0 to vary the integrin-binding status of rat osteoclasts. Rico et al. (28) studied the effects of temperature modification on integrin binding with AFM in leukocytes, but the temperature changes they studied were nonphysiologic, comparing 37°C with 24°C and 17°C. In addition, leukocyte integrins represent a very different pool that is rich in $\beta 2$ subunit heterodimers compared with the heterodimers of $\beta 1$ and $\beta 3$ chiefly expressed by epithelial cells.

In addition, assessments of surface interactions such as binding affinity require large numbers of measurements over random positions. However, commercial AFMs suffer from poor positioning precision for random measurements, since they are built to perform zig-zag scanning tasks. Moreover, the lack of human interface further undermines their capability as a biologically intensive screening and surveying instrument. Thus, we introduced the use of AFM-based nanorobotics for this application by considering the AFM cantilever as a robotic arm (29,30). Equipped with a series of hardware and software upgrades to a commercial AFM, one can position the probe precisely to a desired location with ease using a joystick through a customer-tailored external closed-loop system for random positioning and control. This greatly enhances the measurement capability of AFM, especially when large numbers of measurements are required for statistical analysis (31,32). Here, we use the AFM robotic system to characterize the interaction between RGD-containing peptides and integrins, and assess the binding status in response to different ions, ion-ion interactions, and inhibitors of intracellular kinases. This research allows us to quantify the changes on a nanoscale in a physiologically based process and provide meaningful future applications. We also delineate three distinct states of integrin binding and correlate them with conformational changes proposed in the literature.

MATERIALS AND METHODS

Cell line and cell culture

Caco-2BBE cells are an enterocytically differentiated subclone of the original Caco-2 (33). Previous work from our laboratory demonstrated that Caco-2 cells express $\beta 1$ and $\beta 3$ integrin subunits in combination with the $\alpha 1$, $\alpha 2$, $\alpha 3$, $\alpha 5$, and $\alpha 6$ subunits (2). The peptide used here for binding would be expected to bind reproducibly to integrin heterodimers between the $\beta 1$ subunit and the $\alpha 1$–$\alpha 3$ subunits (34).

Caco-2 cells (ATCC, Manassas, VA) were cultured in Dulbecco's modified Eagle's medium (DMEM; Invitrogen, Carlsbad, CA) supplemented with 10% heat-inactivated fetal bovine serum (Sciencell, Carlsbad, CA), 1% penicillin/streptomycin (Invitrogen), and 10 g/ml transferrin (Sigma-Aldrich, St. Louis, MO) at 37°C in a humidified 5% CO_2 environment. Caco-2 cells between passages 60 and 70 were utilized. The cells were subcultured using 0.05% trypsin-EDTA solution (Invitrogen). The cells were plated on sterilized 1-cm-diameter glass slides prepared by immersion in 12.50 μg/ml type I collagen in enzyme-linked immunosorbent assay (ELISA) buffer (Sigma-Aldrich) overnight at 4°C. Freshly passaged cells were distributed on the glass slides and grown in standard 12-well plates in DMEM until they were 90% confluent.

Tip preparation and coating

AFM tips made of silicon nitride were used in the measurement of integrin affinity. The AFM tip was UV-cleaned for 15 min and then coated with polyethylene glycol (PEG; Sigma-Aldrich, St. Louis, MO) as a linker by immersion in 1 g/ml. Next, the tip was coated in either an RGD peptide (1 mg/mL; Sigma-Aldrich, St. Louis, MO) in Ca^{2+}- and Mg^{2+}-free phosphate-buffered saline (PBS) as the positive test or a glycine-arginine-glycine-glutamate-serine-proline (RGE) peptide (1 mg/ml; AnaSpec, San Jose, CA) in PBS as the control. The AFM tip was immersed in PEG for 20 min, washed three times with PBS, coated with RGD or RGE for 20 min, and then washed three times with PBS.

Cell treatments and cation modulation

Once the Caco-2 cells attained 90% confluence, they were prepared for measurement. Initially, the Caco-2-coated glass slides were washed three times with PBS to remove any residual medium. For cation modulation, the cells were allowed to equilibrate for 5 min in pH-controlled 10 mM HEPES supplemented with either 1 mM Ca^{2+}, 1 mM Mg^{2+}, 1 mM Ca^{2+} with 1 mM Mg^{2+}, or 1 μM of the cation chelator, EDTA. The cells were subsequently measured by AFM using random affinity measurements over cells, as described below.

Intracellular signal modulation

We used 1,2,4,5-benzenetetraamine tetrahydrochloride (Y15; Sigma-Aldrich) to inhibit intracellular FAK, which modulates extracellular integrin-binding affinity. Y15 was diluted in PBS with 1% bovine serum albumin (BSA). The cells were washed three times with warm PBS, pretreated in 1 mM Mg^{2+} in 10 mM HEPES with 20 μM Y15 or Y15 vehicle for 30 min at 37°C, and then measured with AFM as described below.

Global cell adhesion

Purified type I collagen was precoated at saturating densities of 12.50 μl/ml on nontreated 24-well plates using an ELISA-based buffer overnight at 4°C. The plates were washed three times with PBS and equilibrated with 10 mM HEPES/PBS for 30 min prior to the adhesion experiment. After attaining 90% confluence, Caco-2 cells were subcultured into T75 flasks at a concentration of 500,000 cells per flask, and allowed to grow for another 48 hr. The cells were then pretreated in either 10 mM HEPES/PBS with 1 mM Mg^{2+} and 20 μM Y15, 20 μM Y15 only, or Y15 vehicle (PBS 1% BSA) for 30 min at 37°C. After the pretreatment, they were trypsinized (2–3 min) and the trypsin was neutralized with cell culture medium. The cells were then centrifuged and resuspended in 1 μM Calcein-AM (Invitrogen) in

warm PBS and incubated in Calcein for 15 min at 37°C. The cells were centrifuged again and pretreated for 5 min at 37°C in pH-controlled 10 mM HEPES supplemented with either 1 mM Ca^{2+}, 10 mM Ca^{2+}, 1 mM Mg^{2+}, 10 mM Ca^{2+} with 1 mM Mg^{2+}, 1 mM EDTA, or 1 mM Mg^{2+} with 1 mM EDTA. Then 80,000 cells were added to each well and incubated at 37°C for 30 min. They were then washed twice in PBS and read at 495 nm excitation and 519 nm emission.

AFM nanorobotic measurement and force displacement curve processing

All force measurements were performed on a customized Bioscope AFM (Bruker Nano, Santa Barbara, CA). Silicon nitride cantilevers with a spring constant of ~0.06 N/m were used, and each individual probe was calibrated using the thermal tune method to get the exact value of the spring constant. The temperature in the experimental setup was maintained at 37°C by a polyimide film heater, as part of the integrated AFM nanorobotic system, underneath the Petri dish during the measurement. Data were sampled using the AFM robotic system by placing the probe to a random position through a joystick to obtain more than a hundred force-displacement curves within a 10 μm $\times$10 μm area, and then another area was selected to sample. Because the vertical moving speed affects the measurement results, all of the measurements were conducted at a loading rate of 1.2 μm/s. A data-processing routine custom written in MATLAB (The MathWorks, Natick, MA) was utilized to convert the force-displacement curve to an unbinding force by detecting the largest cantilever deflection change in the pull-off phase. The unbinding forces collected were then analyzed statistically to obtain the frequency distribution, which was subsequently fitted with a multi-Gaussian distribution. The distribution pattern was ultimately assessed as an indicator of the integrin adhesion pattern.

Western blot blockade of FAK

FAK inhibition was verified by western blot for FAK (Y397) phosphorylation, a key early step in FAK activation. This was achieved by inducing FAK activation via adhesion to collagen. After 30 min of treatment in either 100 μM Y15 or Y15 vehicle at 37°C, cells were trypsinized and plated on six-well plates precoated with saturating densities of type I collagen. The cells were then incubated at 37°C for 30 min. The adherent cells were then washed with cold PBS. Lysis buffer (50 mM Tris pH 7.4, 150 mM NaCl, 1% TritonX-100, 1% sodium deoxycholate, 0.1% sodium dodecyl sulfate (SDS), 1 mM EDTA, 1 mM phenylmethylsulfonyl fluoride, 1 mM Na3VO4, 50 mM NaF, 10 mM sodium pyrophosphate, 2 μg/ml aprotinin, 2 μg/ml leupeptin, pH 7.4) was added to both cell populations to ensure protein preservation. Protein concentrations in the cell lysates were measured using bicinchoninic acid (BCA) protein. Cell lysates were resolved under reducing conditions by 10% SDS-polyacrylamide gel electrophoresis (SDS-PAGE) before they were transferred to nitrocellulose membranes. Membranes were blotted with antibodies directed against the phosphorylated form of FAK (Y397; Cell Signaling, Beverly, MA) and with the appropriate secondary antibody coupled to horseradish peroxidase. Bands were detected with enhanced chemiluminescence (GE Healthcare, Piscataway, NJ) and analyzed with a Kodak Image Station 440CF (Eastman Kodak, Rochester, NY). All blots were then stripped and similarly reprobed for total FAK. All exposures used for densitometry were within the linear range of the assay.

RESULTS

Detection of single integrin binding force

The affinity measurements of a noncoated AFM probe interacting with the Caco-2 cell surface exhibited a smooth deflection of the cantilever, as can be seen in the withdrawal portion of the representative force-displacement curve in Fig. 1 *A*. The small deflection changes observed over the course of retraction (zoomed in in the *inset* of Fig. 1 *A*) likely reflect the adhesive force between the silicon cantilever and the cell surface as well as the noise of the whole system. An RGE-coated AFM probe produced no distinct unbinding features, although the force displacement curve did show stronger nonspecific interactions between the peptide and the cell membrane, as shown in Fig. 1 *B*. In contrast, the RGD-coated AFM probe withdrawal demonstrated distinct bond rupture events, such as the sudden release of cantilever bending during retraction shown in Fig. 1 *C*. In the representative force curves taken with the RGD-coated AFM probe, the subsequent unbinding of RGD-integrin

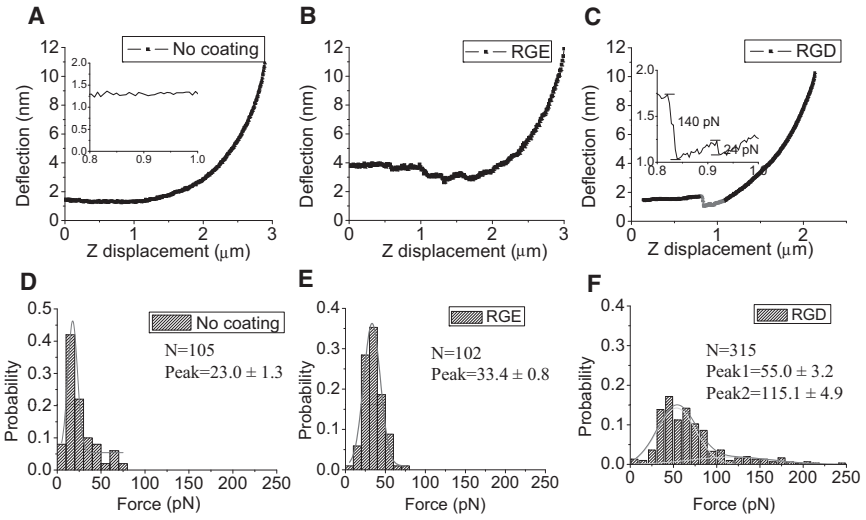

FIGURE 1 No functionalization, nonspecific binding of RGE versus specific binding of RGD. (*A–C*) Single force distance curves between the AFM tip and the surface of individual cells. (*D–F*) Composites of many deflection curves are represented by affinity probabilities; the single deflection curves are representative of all subsequent data. All Caco-2 cells are assessed with affinity dissociations in Ca^{2+}- and Mg^{2+}-free PBS. (*A–C*) Only background noise is measured with a noncoated tip (*A*) or RGE-coated tip (*B*), and a large deflection is noted with RGD coating (*C*). The inset in *C* demonstrates deflection in a stepwise fashion where clusters of integrins sequentially detach from the RGD-coated tip. Large incremental changes are produced by clusters of integrins detaching, and smaller changes are from smaller clusters or individual integrins. As the AFM tip withdraws from the surface of the cell, more and more integrins detach. (*C–E*) Affinity probabilities at varying force levels are characterized with no coating (*C*), RGE coating (*D*), and RGD coating (*E*). (*D–F*) Background noise is seen in (*D*), and nonspecific binding is seen with RGE coating of the AFM probe (*E*), but specific activated binding is observed with RGD binding characterized by the green curve to the right (*F*).

bond(s)/bond clusters are clearly visible. Precise measurement of the retraction reveals 140 pN or 24 pN force changes for the two major stepwise deflections, as shown in the inset of Fig. 1 *C*. Each individual force measurement was location and experiment specific, and the largest rupture events or nonspecific interactions were recorded for each measurement and translated to create affinity probability distributions.

Statistical analysis showed that RGE-coated AFM tips detected a low-deflection-change force-displacement curve when interacting with the cell surface. This was designated nonspecific binding, with a peak value of 33.4 ± 0.8 pN in Fig. 1 *E*. This peak value is higher than the noise level of 23.0 ± 1.3 pN observed using the noncoated AFM tip in Fig. 1 *D*. In contrast, the RGD-coated AFM tip interacting with cell-surface proteins displayed multiple evident unbinding forces, and a similar bell-shaped curve with a peak of 55.0 ± 3.2 pN was observed. Pattern recognition showed a Gaussian distribution and another peak with at 115.1 ± 4.9 pN, as shown in Fig. 1 *F*. This two-peak pattern is designated the specific activated state when the binding site for RGD is in an open status.

We also used covalently bonded RGD sequences to measure the integrin binding force. The covalently bonded probe was functionalized as described previously (35). Briefly, the silicon nitride probe was first UV cleaned and then further cleaned by chloroform. It was then treated with 3-aminopropyltriethoxysilane (APTES) to create the –NH2 on the tip surface. A heterobifunctional PEG linker molecule was then able to bind to the –NH2 with the NHS-ester reactive group. The RGD sequence was modified using N-succinimidyl 3(-acetylthio)propionate (SATP)). The modification enabled the binding of the SATP-labeled sequence to the other end of the PEG linker molecule, maleimide (MAL; illustrated in Fig. 2 *A*; the detailed functionalization protocol can be found in the Supporting Material). The results obtained with this functionalization method (Fig. 2, *B* and *C*) were similar to those obtained by our protocol (26), which uses probes functionalized with PEG as the noncovalent linker through which ligands are passively chemisorbed. Essentially, unbinding forces were detected with the same magnitude as in Fig. 1 *C*. A 118 nN snapshot is shown in Fig. 2 *B* and magnified in the inset. Statistical analysis was also performed on 300 force curves obtained at random positions while Caco-2 cells sat in PBS without Ca^{2+} and Mg^{2+}, the same condition as described in the previous paragraph (Fig. 1, *D–F*). A specific binding interaction peak was clearly observed at ~105 nN (Fig. 2 *C*), similar with that shown in Fig. 1 *F*.

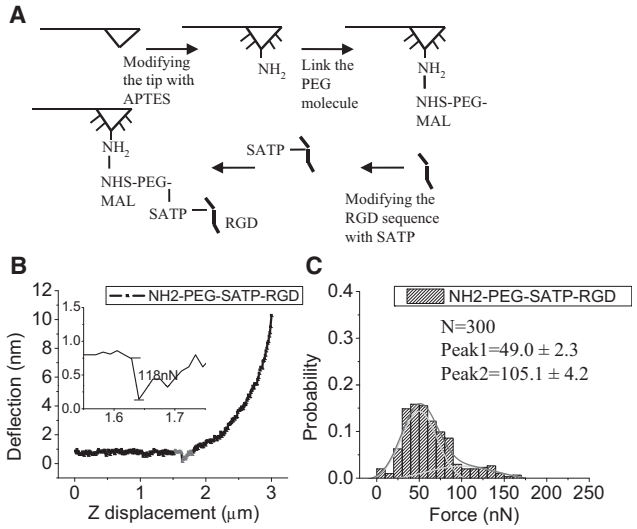

FIGURE 2 Covalent-bond-based functionalization yields a similar result. (*A*) A schematic diagram shows the linking process of the RGD sequence with PEG as crosslinker; the NHS end attaches to the NH_2 group on the cantilever, and the MAL group at the other end links the SATP-modified RGD sequence. (*B*) Representative single force distance curves using covalent-bond-based functionalization shows unbinding activities of similar magnitude in Ca^{2+}- and Mg^{2+}-free PBS. The inset shows the magnified unbinding event. (*C*) Statistical analysis of binding activity with 300 force curves shows a specific peak of ~105 pN.

Cationic modulation of integrin affinity

Adding Ca^{2+} or Mg^{2+} altered the affinities for RGD interaction with the cell membrane. As a control, EDTA chelation allowed us to measure the integrin-binding force probabilities in the absence of divalent extracellular cations. Cationic chelation yielded a baseline level of interaction force of 65.8 ± 2.5 pN (Fig. 3 *A*). We designated this single peak interaction in an ion-free environment as the specific inactivated state of integrin binding. With addition of Ca^{2+} (1 mM), the binding force was subtly lower than that of the EDTA control shown in Fig. 3 *B*, with 56.7 ± 2.0 pN, indicating the capability of this cation in the downregulation of integrin binding to make a specific inactivated state. Addition of Mg^{2+} (1 mM) demonstrated two Gaussian distribution curves, resulting in a higher average binding force measurement with two peaks at 50.1 ± 1.1 and 98.9 ± 3.6 pN, respectively (Fig. 3 *C*), a signature of a specific activated status. When Ca^{2+} and Mg^{2+} were combined at 1 mM each, the binding force remained at baseline measurements (Fig. 3 *D*), with the curve peak at 45.8 ± 1.5 pN. This is a sign that Ca^{2+} overtakes Mg^{2+} in the regulation of integrin, leading to a change in integrin configuration toward a specific inactivated status.

Quantitating cell adhesion to the type I collagen substrate demonstrated similar findings on a global level. The EDTA solution acted as control with the baseline measurements of cell adhesion. Ca^{2+} at 1 mM showed a marginal increase in cell adhesion that was not statistically different from the EDTA control ($p = 0.726$). Mg^{2+} significantly increased the number of remaining cells 2.3-fold compared with cation chelation with EDTA ($p < 0.001$) or Ca^{2+} treatment ($p < 0.001$). Finally, Ca^{2+} and Mg^{2+} together at 1 mM had a significantly increased number of

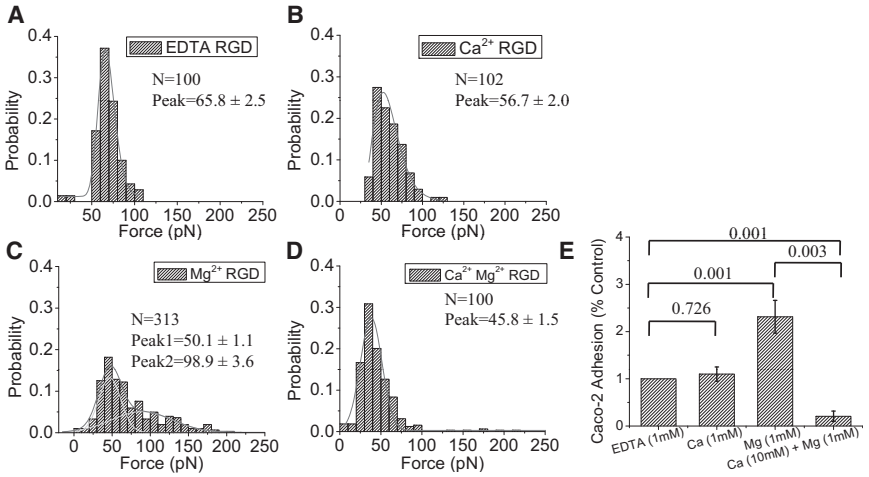

FIGURE 3 Cation-modulation of integrin affinity for RGD. Caco-2 cells were investigated with an RGD-coated probe in varying ion-containing HEPES solutions to develop affinity probability curves. (*A*) The cation-chelating agent EDTA in HEPES solution demonstrates nonspecific binding when investigated with average binding force of 65.8 ± 2.5 pN. (*B*) The affinity curve has a slight rightward shift with higher binding force values than ion chelation of 56.7 ± 2.0 pN, creating a specific inactivated binding with 1 mM Ca^{2+} HEPES solution. (*C*) Specific activated integrin binding is demonstrated with 1 mM Mg^{2+} HEPES solution with a separate curve above baseline measurements fitted with the green line at 98.9 ± 3.6 pN. (*D*) The specific activated binding of 1 mM Mg^{2+} is antagonized when 1 mM Ca^{2+} is present in the HEPES solution with a return to specific inactivated, or ion-chelated levels. Global adhesion of Caco-2 cells in the same ion conditions as in *A–D* demonstrates a nonsignificant increase in adhered cells to type I collagen substrate in Ca^{2+}, a significant 2.3× increase in adhesion with Mg^{2+}, and a significant 0.2× decrease in adherent cells with Ca^{2+} and Mg^{2+} together compared with EDTA control (*E*).

remaining cells, similar to Mg^{2+} alone ($P < 0.001$), but was nonsignificantly lower than Mg^{2+} alone ($p = 0.631$; data not shown). In contrast, a 10 mM Ca^{2+} with 1 mM Mg^{2+} caused a significantly decreased number of adherent cells compared with EDTA ($p < 0.001$), Mg^{2+} ($p = 0.003$), or 1 mM Ca^{2+} ($p = 0.005$). These results are summarized in Fig. 3 *E*.

Intracellular integrin regulation

Mg^{2+} produced two Gaussian distribution curves similar to those shown Fig. 3 *C* when the Y15 vehicle was present (Fig. 4 *A*), but the higher binding-affinity curve was abrogated by Y15. Mg^{2+} created an increase in the average binding force of integrins to 103.6 ± 3.7 pN, whereas Y15 prevented this change and produced a distribution of affinity probabilities near baseline values and at the same value as the lower peak of Mg^{2+} with 52.3 ± 2.1 pN (Fig. 4 *B*). This is similar in fashion to the Ca^{2+} and Mg^{2+} combination in Fig. 3 *D*, where the integrins are at the specific inactivated status. Overall, the cell adhesion studies showed similar results, i.e., Mg^{2+} caused a 2.3-fold increased number of cells to remain attached after treatment, which is significantly higher than the EDTA-control ($p < 0.001$). In addition, Y15 nonsignificantly reduced the attachment of cells as compared with Mg^{2+} with Y15 vehicle ($p = 0.347$), but still possessed a significantly higher value than the EDTA control ($p < 0.001$), as shown in Fig. 4 *C*. Y15's ability to alter FAK phosphorylation was verified by western blot. After 100 μM Y15 treatment, adherent cells possessed a significantly decreased amount of phosphorylated FAK as compared with the control cells exposed only to Y15 vehicle ($p = 0.01$). The results of the FAK-blocking western blot can be seen in Fig. 5, *A* and *B*.

DISCUSSION

In this study, we measured on an individual level (rather than a global level) the force of attraction between individual integrin heterodimers and RGD hexapeptide. We

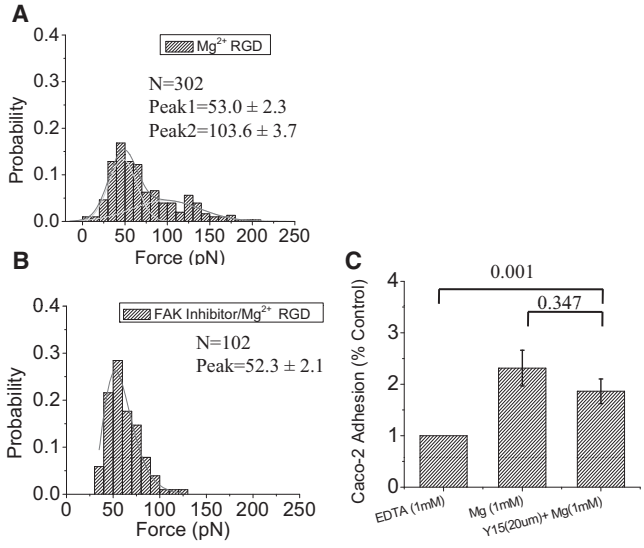

FIGURE 4 FAK modulation of integrin affinity for RGD. (*A* and *B*) Affinity probability curves were developed for Caco-2 cells probed with an RGD-coated tip in 1 mM Mg^{2+} HEPES solution and Y15 vehicle (*A*) or 20 μM Y15 (FAK inhibitor) pretreatment (*B*). With the vehicle, measurements demonstrate specific-activated binding of RGD-integrin interactions, fit with the green curve at 103.6 ± 3.7 pN. However, pretreatment with Y15 only shows specific inactivated integrin binding interactions with RGD at 52.3 ± 2.1 pN. Similarly to AFM measurement, global cell adhesion measured the integrin affinity of whole cells for the type I collagen substrate. (*C*) Compared with the EDTA control, Mg^{2+} significantly increased the number of cells that were able to adhere to the substrate 2.3×, and Y15 nonsignificantly decreased the ability of Mg^{2+}-treated cells to adhere. The Y15 treatment was 1.8× higher than the EDTA control.

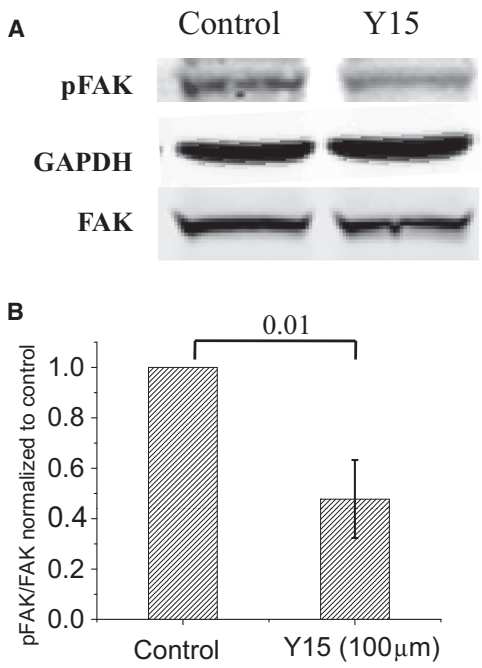

FIGURE 5 Western blot of FAK inhibition. The FAK-specific inhibitor Y15 prevented pressure-induced increases in Caco-2 FAK (Y397) phosphorylation. Protein samples from the lysates of Caco-2 cells treated with 100 μM Y15 or control (Y15 vehicle) were directly analyzed by western blot using phospho-specific antibody to FAK (Y397), as well as antibodies to FAK. GAPDH was used as a loading control. (*A*) Typical blots. (*B*) Graph summarizing the densitometric analyses of the ratio of FAK (Y397) phosphorylation to total FAK. The level of phosphorylated FAK (pFAK) was significantly lower in adherent cells with Y15 treatment compared with the adherent cells of the control group ($n = 7$, $^*P = 0.01$). All observations were normalized against control cells.

objectively defined three integrin-binding states: nonspecific, specific inactivated, and specific activated. Furthermore, we demonstrated directly that both extracellular cations and intracellular signaling events can specifically modulate individual integrin heterodimer binding affinity. The latter, in particular, has only previously been inferred from indirect evidence (12,36). Finally, our Y15 experiments provide proof of principle that integrin-binding affinity can be directly modulated in intact cells by treatment with a small-molecule inhibitor.

Lehenkari and Horton's (26) estimate of the binding affinity of a single RGD-integrin interaction was between 30 and 40 pN, whereas our calculations in a controlled environment yielded a binding force of 46 $\pm$ 4.1 pN. Although it is similar in magnitude, their estimate is 2–3 SDs different from the binding force we measured. This apparent difference may be due to the overall system that was employed for the experiment. We used an AFM-based nanorobotic system with human-directed precision control to reach any part of the cell, whereas ordinary AFM systems limit measurements to the spread cell edges. Furthermore, the human interface via a joystick enables us to survey a greater number of points covering a larger area, which will effectively yield reliable results in situations with nonuniformly distributed integrin receptors. Certainly, it could also be due to the calibration of the cantilever spring constants and AFM detector sensitivity. The differences in individual integrins and cells may affect cell signaling and cellular structures, and thus cause variation in the measurements as well.

The result obtained using the covalent-bond functionalized probe matches well with that obtained using the chemisorbing method, proving the validity of the measurement result. Similar unbinding forces were recorded using both methods. The fact that we were able to detect interaction forces comparable to other published results, and observed distinct force values demonstrates that the measured force should represent bond breaking of the receptor-ligand interaction, rather than forces uprooting the receptor from the membrane or dissociating PEG and ligand. Furthermore, the fact that we were not able to detect any significant interaction with the control sequence (RGE), and could modulate the force by different cation conditions and internal cell signaling also reinforces the proposition. Thus, to simplify the process and reduce variability introduced by additional treatment reagents and processes, we used the protocol reported by Lehenkari and Horton (26) throughout the whole experiment, and were able to reproduce this key result a great number of times.

We were able to control for nonspecific protein-lipid and protein-protein interactions using the uncoated AFM tip and RGE substitution, respectively. The RGE substitution is a common control for RGD-related binding (37). Nevertheless, integrins tend to cluster in the cell membrane into focal adhesions, acting together to alter avidity (38), and the AFM likely interacted with many such integrins at once. Observations of large incremental drops in adhesive force are due to the disengagement of bigger groups of integrin-RGD interfaces, whereas small changes correlate with smaller clusters of integrin-RGD interaction detachment. Analysis of the intervals of detachment in each withdrawal of the AFM defines a lowest common denominator representing the amount of force of one RGD-integrin interaction.

The bell-shaped distribution of our affinity measurements requires further comment. There are many different integrin heterodimers that display a wide range of properties and functions. Each heterodimer is composed of different protein structures that may affect the affinity of RGD-integrin binding (5). Because RGD has been shown to bind to several heterodimers (5), it is likely that we interacted with more than one subtype. Therefore, our current results likely reflect the engagement force of the entire collection of integrins present in Caco-2 cells that can bind to RGD peptides. Furthermore, our use of random surface sampling with the AFM probe means it is equally likely that we encountered the center of the cell versus the periphery. To elaborate, focal adhesions have a location-dependent composition (39). For instance, a given focal adhesion complex may have different integrin heterodimer combinations at the

cell edges compared with the body of the cell, leading to a difference in binding values. These factors likely contributed to the Gaussian distribution of binding affinities in our results.

EDTA and Ca^{2+} produced similar but differently distributed baseline binding force curves, suggesting that they suppress full integrin-RGD interactions. Mg^{2+} supplementation yielded a large, rightward-shifted binding curve. This is consistent with the concept that occupation of the divalent cation-binding site on the extracellular domain of the $\beta 1$ integrin subunit by magnesium cations can alter integrin tertiary and quaternary structure to expose or enhance the binding affinity of the RGD-binding site jointly specified by both the β and α integrin subunits (3,40). Adding Ca^{2+} along with Mg^{2+} suppressed this rightward shift; in this case, Ca^{2+} acted as an antagonist of Mg^{2+}. Our global assays of cell adhesion used 10 mM Ca^{2+} with 1 mM Mg^{2+} instead of 1 mM Ca^{2+} because we were not able to demonstrate a statistically significant decrease with 1 mM Ca^{2+}. In contrast, the AFM measurements were more sensitive and were able to detect significant antagonism between 1 mM Ca^{2+} and 1 mM Mg^{2+} together. This suggests that the AFM technique is sensitive for measuring effects on these nanoscale forces of protein-protein interactions.

Y15 blocks FAK phosphorylation and its consequent activation, and has been reported to decrease cell attachment to its substrate (17). FAK inhibition by Y15 was able to modulate the affinity of individual integrins. Indeed, Y15 inhibited the second binding peak that Mg^{2+} promotes. FAK activity is classically modulated by integrin signaling after engagement with matrix proteins (41), but our results clearly define the other side of a feedback loop in which FAK in turn modulates integrin-binding affinity for the ECM.

Despite the heterogeneity and distribution of the integrins, we were able to manipulate the status of the integrins expressed by the cells together, as evidenced by the overall rightward shift in the curve distribution, and the three states of integrin binding that could be achieved (nonspecific, specific inactivated, and specific activated). Our ion-chelation studies demonstrated nonspecific binding of the RGD-coated AFM tip with the cell. The studies with Ca^{2+} treatment or the FAK inhibitor demonstrated a specific inactivated binding state of integrins, whereas the studies with Mg^{2+} supplementation demonstrated specific activated integrin binding. Importantly, different conformations of the integrin may still bind ligands such as RGD, even in the closed state (42,43). Different ions and intracellular signals are known to change the conformation of integrins (38,44). Therefore, we actually bound integrins in different states and measured the properties in these critically important conditions. This is consistent with previous studies suggesting that multiple forms of integrin conformation lead to ligand affinity changes (44). In addition, the overall breaking point of the integrin-RGD interactions varies depending on the number of integrins that are bound to the tip: the single integrin-binding force, determined statistically, differed among the three states. Each state had a different individual binding force that correlated with the curve distributions. The number of clusters that unbound in stepwise fashion, however, did not have a discernible pattern among the integrin states.

Understanding these molecular-level forces may allow us to further understand and evaluate a cell's interaction with its environment. Furthermore, this allows for molecular and global studies in this field combined with a clinical setting, as cations have been shown to affect colon cancer and adhesion (45). In addition, FAK has been implicated in cancer states, and treatments are currently being explored (46,47). Future directions include the exploration of integrin affinity modulation in the context of disease states. It will be especially important to explore changes on the individual integrin level that lead to a global cell change, which will allow us to understand the nature of cell-ECM interactions. The in situ screening of live cells enabled by the AFM-based nanorobot could be an important tool for elucidating how cells adhere in vivo during processes as diverse as developmental migration, inflammation, and metastasis.

SUPPORTING MATERIAL

Protocol for NHS-PEG-MAL peptide Functionalization is available at http://www.biophysj.org/biophysj/supplemental/S0006-3495(13)00640-1.

The authors thank C. Su from Bruker-Nano Inc. for technical advice regarding the equipment used in this study.

This work was supported by National Science Foundation grants IIS-0713346 and DMI-0500372, Office of Naval Research grants N00014-04-1-0799 and N00014-07-1-0935, and National Institutes of Health grants R43 GM084520 and RO1DK060771.

REFERENCES

1. Kawauchi, T. 2012. Cell adhesion and its endocytic regulation in cell migration during neural development and cancer metastasis. *Int. J. Mol. Sci.* 13:4564–4590.
2. Wehrle-Haller, B., and B. A. Imhof. 2003. Integrin-dependent pathologies. *J. Pathol.* 200:481–487.
3. Hynes, R. O. 2002. Integrins: bidirectional, allosteric signaling machines. *Cell.* 110:673–687.
4. Zhang, J. H., W. Li, …, M. D. Basson. 2003. Regulation of the intestinal epithelial response to cyclic strain by extracellular matrix proteins. *FASEB J.* 17:926–928.
5. Takada, Y., X. J. Ye, and S. Simon. 2007. The integrins. *Genome Biol.* 8:215.
6. Xiong, J. P., T. Stehle, …, M. A. Arnaout. 2002. Crystal structure of the extracellular segment of integrin α Vβ3 in complex with an Arg-Gly-Asp ligand. *Science.* 296:151–155.
7. Humphries, J. D., A. Byron, and M. J. Humphries. 2006. Integrin ligands at a glance. *J. Cell Sci.* 119:3901–3903.
8. Ruoslahti, E. 1996. RGD and other recognition sequences for integrins. *Annu. Rev. Cell Dev. Biol.* 12:697–715.

9. Shimaoka, M., J. Takagi, and T. A. Springer. 2002. Conformational regulation of integrin structure and function. *Annu. Rev. Biophys. Biomol. Struct.* 31:485–516.
10. Thamilselvan, V., M. Fomby, …, M. D. Basson. 2003. Divalent cations modulate human colon cancer cell adhesion. *J. Surg. Res.* 110: 255–265.
11. Weinreb, P. H., S. Li, …, V. L. Woods, Jr. 2012. Dynamic structural changes are observed upon collagen and metal ion binding to the integrin α1 I domain. *J. Biol. Chem.* 287:32897–32912.
12. Craig, D. H., C. P. Gayer, …, M. D. Basson. 2009. Increased extracellular pressure enhances cancer cell integrin-binding affinity through phosphorylation of β1-integrin at threonine 788/789. *Am. J. Physiol. Cell Physiol.* 296:C193–C204.
13. van Kooyk, Y., and C. G. Figdor. 2000. Avidity regulation of integrins: the driving force in leukocyte adhesion. *Curr. Opin. Cell Biol.* 12:542–547.
14. Jones, R. J., V. G. Brunton, and M. C. Frame. 2000. Adhesion-linked kinases in cancer; emphasis on src, focal adhesion kinase and PI 3-kinase. *Eur. J. Cancer.* 36(13 Spec No):1595–1606.
15. Zhao, X., and J.-L. Guan. 2011. Focal adhesion kinase and its signaling pathways in cell migration and angiogenesis. *Adv. Drug Deliv. Rev.* 63:610–615.
16. van Nimwegen, M. J., and B. van de Water. 2007. Focal adhesion kinase: a potential target in cancer therapy. *Biochem. Pharmacol.* 73:597–609.
17. Golubovskaya, V. M., C. Nyberg, …, W. G. Cance. 2008. A small molecule inhibitor, 1,2,4,5-benzenetetraamine tetrahydrochloride, targeting the y397 site of focal adhesion kinase decreases tumor growth. *J. Med. Chem.* 51:7405–7416.
18. Schaller, M. D. 2010. Cellular functions of FAK kinases: insight into molecular mechanisms and novel functions. *J. Cell Sci.* 123:1007–1013.
19. Playford, M. P., and M. D. Schaller. 2004. The interplay between Src and integrins in normal and tumor biology. *Oncogene.* 23:7928–7946.
20. Jung, S. H., D. Park, …, K. S. Ha. 2010. Molecular imaging of membrane proteins and microfilaments using atomic force microscopy. *Exp. Mol. Med.* 42:597–605.
21. Kim, I. H., M. N. Lee, …, J. W. Park. 2011. Nanoscale mapping and affinity constant measurement of signal-transducing proteins by atomic force microscopy. *Anal. Chem.* 83:1500–1503.
22. Fung, C. K. M., K. Seiffert-Sinha, …, A. A. Sinha. 2010. Investigation of human keratinocyte cell adhesion using atomic force microscopy. *Nanomedicine.* 6:191–200.
23. Chen, Y., G. C. Zeng, …, Z. W. Chen. 2011. AFM force measurements of the gp120-sCD4 and gp120 or CD4 antigen-antibody interactions. *Biochem. Biophys. Res. Commun.* 407:301–306.
24. Gunning, A. P., S. Chambers, …, C. Nicoletti. 2008. Mapping specific adhesive interactions on living human intestinal epithelial cells with atomic force microscopy. *FASEB J.* 22:2331–2339.
25. Sun, Z., L. A. Martinez-Lemus, …, G. A. Meininger. 2005. Mechanical properties of the interaction between fibronectin and $\alpha 5\beta$1-integrin on vascular smooth muscle cells studied using atomic force microscopy. *Am. J. Physiol. Heart Circ. Physiol.* 289:H2526–H2535.
26. Lehenkari, P. P., and M. A. Horton. 1999. Single integrin molecule adhesion forces in intact cells measured by atomic force microscopy. *Biochem. Biophys. Res. Commun.* 259:645–650.
27. Mahabeleshwar, G. H., J. H. Chen, …, T. V. Byzova. 2008. Integrin affinity modulation in angiogenesis. *Cell Cycle.* 7:335–347.
28. Rico, F., C. Chu, …, V. T. Moy. 2010. Temperature modulation of integrin-mediated cell adhesion. *Biophys. J.* 99:1387–1396.
29. Xi, N., C. K. M. Fung, …, L. Q. Liu. 2011. Atomic force microscopy as nanorobot. *Methods Mol. Biol.* 736:485–503.
30. Li, G., N. Xi, and D. H. Wang. 2005. In situ sensing and manipulation of molecules in biological samples using a nanorobotic system. *Nanomedicine.* 1:31–40.
31. Yang, R., N. Xi, …, D. H. Wang. 2012. Cellular biophysical dynamics and ion channel activities detected by AFM-based nanorobotic manipulator in insulinoma β-cells. *Nanomedicine.* S1549-9634:00608–00609.
32. Yang, R. G., N. Xi, …, D. H. Wang. 2011. Nanomechanical analysis of insulinoma cells after glucose and capsaicin stimulation using atomic force microscopy. *Acta Pharmacol. Sin.* 32:853–860.
33. Peterson, M. D., and M. S. Mooseker. 1992. Characterization of the enterocyte-like brush border cytoskeleton of the C2BBe clones of the human intestinal cell line, Caco-2. *J. Cell Sci.* 102:581–600.
34. Basson, M. D. 1992. Regulation of intestinal mucosal healing by growth factors and matrix proteins: a cell culture model. PhD thesis. Yale University, New Haven, CT.
35. Stroh, C., H. Wang, …, P. Hinterdorfer. 2004. Single-molecule recognition imaging microscopy. *Proc. Natl. Acad. Sci. USA.* 101:12503–12507.
36. Craig, D. H., C. R. Owen, …, M. D. Basson. 2008. Colchicine inhibits pressure-induced tumor cell implantation within surgical wounds and enhances tumor-free survival in mice. *J. Clin. Invest.* 118:3170–3180.
37. Hautanen, A., J. Gailit, …, E. Ruoslahti. 1989. Effects of modifications of the RGD sequence and its context on recognition by the fibronectin receptor. *J. Biol. Chem.* 264:1437–1442.
38. Wehrle-Haller, B. 2012. Structure and function of focal adhesions. *Curr. Opin. Cell Biol.* 24:116–124.
39. Welf, E. S., U. P. Naik, and B. A. Ogunnaike. 2011. Probabilistic modeling and analysis of the effects of extra-cellular matrix density on the sizes, shapes, and locations of integrin clusters in adherent cells. *BMC Biophys.* 4:15.
40. Gotwals, P. J., G. Chi-Rosso, …, V. Koteliansky. 1999. Divalent cations stabilize the α1 β1 integrin I domain. *Biochemistry.* 38:8280–8288.
41. Raghavan, S., A. Vaezi, and E. Fuchs. 2003. A role for $\alpha\beta$1 integrins in focal adhesion function and polarized cytoskeletal dynamics. *Dev. Cell.* 5:415–427.
42. Sarantos, M. R., S. Raychaudhuri, …, S. I. Simon. 2005. Leukocyte function-associated antigen 1-mediated adhesion stability is dynamically regulated through affinity and valency during bond formation with intercellular adhesion molecule-1. *J. Biol. Chem.* 280:28290–28298.
43. Adair, B. D., J. P. Xiong, …, M. Yeager. 2005. Three-dimensional EM structure of the ectodomain of integrin αVβ3 in a complex with fibronectin. *J. Cell Biol.* 168:1109–1118.
44. Takagi, J., B. M. Petre, …, T. A. Springer. 2002. Global conformational rearrangements in integrin extracellular domains in outside-in and inside-out signaling. *Cell.* 110: 599–11.
45. van der Voort van Zyp, J., W. C. Conway, …, M. D. Basson. 2005. Divalent cations influence colon cancer cell adhesion in a murine transplantable tumor model. *Am. J. Surg.* 190:701–707.
46. Dunn, K. B., M. Heffler, and V. M. Golubovskaya. 2010. Evolving therapies and FAK inhibitors for the treatment of cancer. *Anticancer. Agents Med. Chem.* 10:722–734.
47. Thamilselvan, V., D. H. Craig, and M. D. Basson. 2007. FAK association with multiple signal proteins mediates pressure-induced colon cancer cell adhesion via a Src-dependent PI3K/Akt pathway. *FASEB J.* 21:1730–1741.